1   **Influence of Solar Irradiation on Nitrous Acid Production in Western U.S. Wildfire Smoke**

2   **J. H. Kaspari[1], J. Chai[2], B. E. Anderson[3], C. E. Jordan[3,4], E. Scheuer[5], M. G. Hastings[2] and**
3   **J. E. Dibb[5]**

4   (1) Department of Chemistry, University of New Hampshire, Durham, NH, USA, (2)
5   Department of Earth, Environmental and Planetary Sciences, and Institute at Brown for
6   Environment and Society, Brown University, Providence, RI, USA, (3) NASA Langley Research
7   Center, Hampton, VA, USA, (4) National Institute of Aerospace, Hampton, VA, USA,
8   (5) Institute for the Study of Earth, Ocean, and Space, University of New Hampshire, Durham,
9   NH, USA.

10   Corresponding author: Jackson Kaspari (jhk2000@wildcats.unh.edu)

11   ORCID ID: 0000-0003-2827-4989

12   **Key Points:**

13   • Strong evidence for substantial daytime and nocturnal secondary production of nitrous
14   acid in biomass burning plumes.

15   • Daytime conversion of nitrogen dioxide to nitrous acid more than compensated for rapid
16   photolytic losses of HONO in Williams Flats fire.

17   • Ground surfaces likely provide the dominant surface area for the heterogenous secondary
18   production of HONO.

19

20   **Abstract**

21   Biomass burning is a primary emission source for a host of gas- and aerosol-phase

22   compounds, which can damage environmental and human health. During the FIREX-AQ

23   campaign in July and August of 2019, we measured reactive nitrogen species (NO_x, NO_2,

24   HONO, HNO_3 and p-NO_3^-), in wildfire plumes aboard NASA Langley's Mobile Aerosol

25   Characterization Laboratory (MACH-2). Nitrous acid (HONO) and nitric acid (HNO_3) mixing

26   ratios were measured at nominal 5-minute resolution using a dual mist chamber-ion

27   chromatograph from five separate areas of fire in the western US and are the primary focus of

28   this paper. Average HONO mixing ratios were significantly higher in young daytime smoke

29   compared to young nighttime smoke, while no statistical differences were observed between

30   young versus aged smoke during the day or night. In the largest fire sampled during the day, UV-

31   A irradiation was highly correlated ($R^2 = 0.91$) with HONO to nitrogen dioxide (NO_2) ratios

32   indicating that photo-enhanced heterogeneous NO_2 to HONO conversion, likely facilitated by

33   ground surfaces (e.g. soil, foliage, and dust), more than compensated for rapid photolytic loss of

34   HONO.

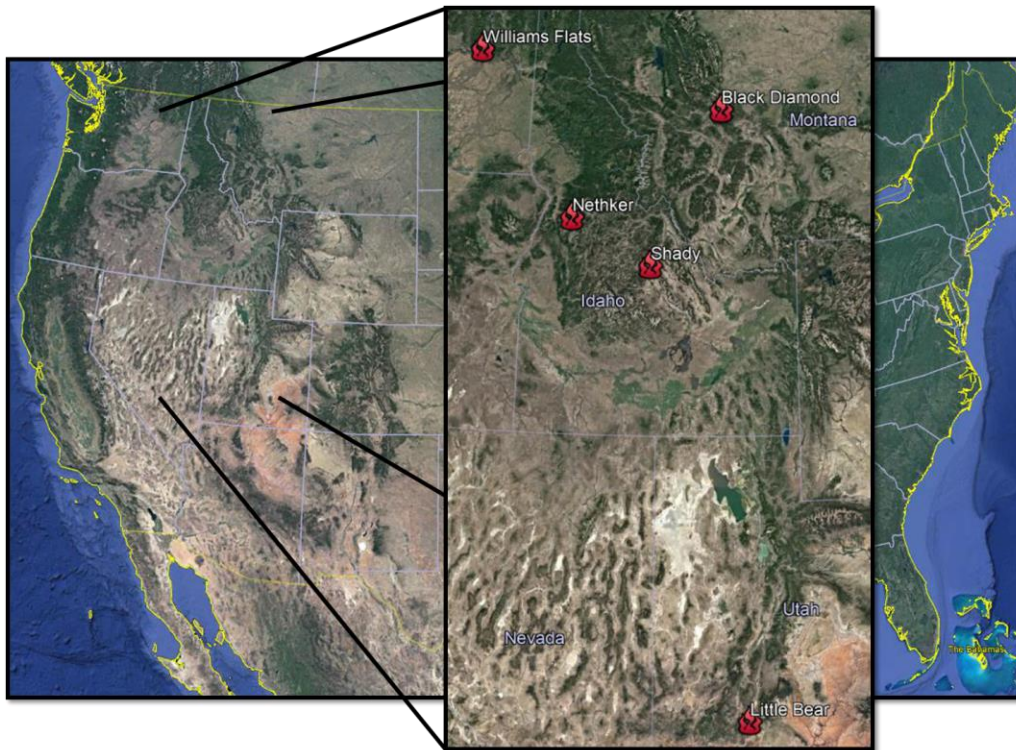35   **Plain Language Summary**

36   Wildfires negatively impact environmental and human health. Reactive nitrogen pathways are

37   complex and research questions still remain regarding the formation of nitrous acid (HONO) in

38   wildfire plumes. Our observations show that HONO can be made in a smoke plume, even as that

39   smoke plume ages and mixes with surrounding air in both the daytime and nighttime. During the

40   day sunlight rapidly destroys HONO but our data suggests that HONO is being made faster than

41   it is lost in smoke close to the land surface. Moreover, the HONO is being produced by the

42   combination of nitrogen dioxide (NO_2) on surfaces such as soil, leaf foliage and dust.

43
44
45
46
47
48
49
50
51
52
53

1. Introduction

54

55   Biomass burning (BB) is a primary emission source for a multitude of gas- and aerosol-phase

56   compounds that impact environmental and human health (Grutzen & Andreae, 1990). Climate

57   change induced global temperature increases have resulted in rises in the total acreage burned in

58   the Western United States (Hoover & Hanson, 2019). A single degree centigrade of warming is

59   predicted to result in a two to four times increase in burned areas (Warneke et al., 2015). The

60   pressing need to better understand BB impacts on air quality and climate has motivated a number

61   of recent collaborative field campaigns including the Studies of Emissions, Atmospheric

62   Composition, Clouds and Climate Coupling by Regional Surveys (SEAC[4]RS); the fourth Fire

63   Lab at Missoula Experiment (FLAME-4); the Fire Influence on Regional to Global

64   Environments Experiment Fire Lab (FIREX-FIRELAB); Western wildfire Experiment for Cloud

65   chemistry, Aerosol absorption and Nitrogen (WE-CAN); and the Fire Influence on Regional to

66   Global Environments Experiment-Air Quality Campaign (FIREX-AQ) during which the data for

67   this paper were collected. FIREX-AQ addressed four main research topics: the dependence of

68   emissions on fuel sources, the difference in emissions between flaming and smoldering fires, the

69   mode of atmospheric transport of smoke plumes, and how plumes compositionally change as

70   they age (ESRL Chemical Sciences Division, 2019).

71   During FIREX-AQ collaborators from UNH, NASA Langley Aerosol Research Group

72   Experiment (LARGE), and Brown University deployed NASA Langley's Mobile Aerosol

73   Characterization Laboratory (MACH-2) during July and August of 2019 to measure the

74   compositional and microphysical properties of smoke in the vicinity of active forest fires.

75   Daytime and nighttime measurements were taken at the Shady, Black Diamond, Williams Flats,

76   Nethker and Little Bear fires which spanned four states (Idaho, Montana, Washington and Utah)

77   in the western U.S (Figure 1). Access to these fires varied depending on the availability of roads

78   as well as safety concerns, but in all cases, sampling was performed at the closest allowable

79   locations. MACH-2 is capable of stationary and mobile sampling, with stationary sampling

80   preferred as it limited issues with instrumentation caused by rough road conditions as well as

81   potential interference from sampling anthropogenic roadway emissions. However, the lofted

82   nature of most wildfire smoke plumes during the daytime required sampling while driving to

83   locations where smoke from the Williams Flats and Nethker fires was mixed down to the ground.

84   Most nighttime sampling was conducted while MACH-2 was parked in locations where it was

85   anticipated that smoke would settle into nearby valleys as fire intensity was lower than during

86   late afternoon peak fire activity.

87

88   Figure 1. Locations of fires sampled by MACH-2 during FIREX-AQ.

89   This work examines the observed mixing ratios of nitrous acid (HONO), nitric acid

90   (HNO$_3$), and particulate nitrate to establish the daytime and nighttime formation pathways and

91   oxidative products of nitrogen oxides (NO$_x$). HONO and NO$_x$ are of particular importance

92   because their reactivity with other atmospheric species result in a net production of ozone (O$_3$) in

93   the troposphere (Platt et al., 1980). Tropospheric O$_3$ is an oxidant and potent greenhouse gas that

94   negatively impacts environmental and human health (Seinfeld & Pandis, 2016.). Enhanced O$_3$

95   results in reduced photosynthesis and growth of vegetation, impairing the resiliency of

96   ecosystems (Ainsworth et al., 2012). In humans, O$_3$ can cause muscle constrictions in airways

97   leading to trapped air in the alveoli. Limited exposure thus makes breathing more difficult and

98   results in inflammation and potential damage to airways. Prolonged exposure may result in more

99   serious conditions such as lung disease, chronic obstructive pulmonary disease and aggravation

100   of asthma (Nuvolone, Petri, & Voller, 2018).

101   Daytime reactions of HONO and HNO$_3$ are summarized in Figure 2. Hydroxyl radicals (OH)

102   initially produced from the photolysis of HONO and O$_3$ (not shown) play a central role in the

103   photocyclization of HONO and formation of HNO_3. Isotopic results from the 2016 FIREX-

104   FIRELAB study show that at moderate combustion temperatures (~700 °C) the most preferable

105   nitrogen reaction pathway post NO formation from BB is NO to NO_2 to HONO shown in light

106   blue in Figure 2 (Chai et al., 2019). This reaction pathway is initiated via the reaction of NO with

107   O_3 to form NO_2. NO_2 can then participate in a surface catalyzed heterogeneous reaction to form

108   HONO which then is photolyized back to NO. These surface catalyzed reactions, such as those

109   fostered by quinone species in soil, occur regardless of the presense of solar radiation but are

110   enhanced during solar flux periods (Scharko et al., 2017). While NO_x cyclization occurs, NO also

111   reacts with OH forming HONO which rapidly photolyzes back to NO and OH (George et al.,

112   2015). Peroxy radicals (HO_2 and RO_2) formed from the oxidation of volatile organic compounds

113   form NO_2 from NO without consuming O_3 and thus lead to a net production of O_3 (George et al.,

114   2015). HNO_3 is formed when NO_2 reacts with OH and serves as a major sink for NO_x as it is

115   removed from the atmosphere by wet and dry deposition relatively rapidly (Adon et al., 2013;
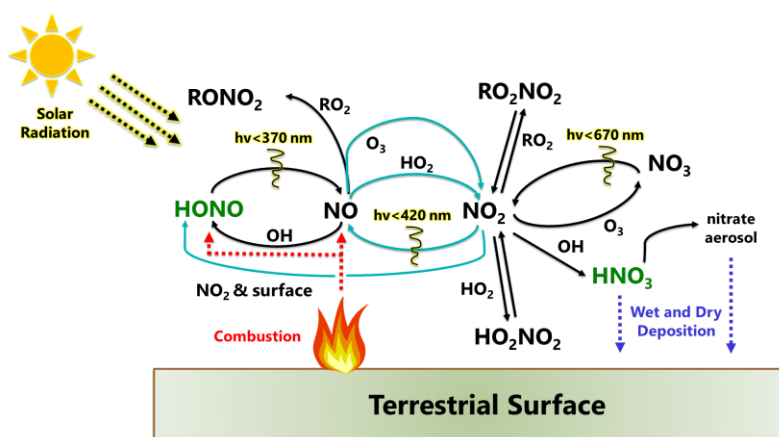
116   Ossohou et al., 2019).

117
118   Figure 2. Summary of daytime pathways for reactive nitrogen in smoke plumes. Light blue arrows indicate the
119   preferred pathway for HONO production under moderate combustion temperatures.
120

121   Less is known about nighttime reactions involving HONO and HNO_3. At night, plumes settle

122   down into the boundary layer and have major impacts on air quality close to the terrestrial

123   surface. This provides a chance for ground-based mobile lab measurements to collect data

124   inaccessible to airborne platforms due to nighttime flight restrictions and proximity of the plume

125   to the ground. At night the lack of solar radiation ceases photolysis and therefore halts the NO_x

126   cycling between NO and NO_2 (Figure 3). This generally leads to increasing concentrations of

127   HONO until dawn when photolysis starts back up (Stutz et al., 2004). As the nighttime NO_x sink

128   occurs again via wet and dry deposition, these nitrate aerosols stem from the formation of NO_3

129   radicals via reaction of NO_2 with O_3, which can further react with NO_2 forming dinitrogen

130   pentoxide (N_2O_5) (Brown & Stutz, 2012). Water on the surface of aerosol reacts with N_2O_5 to

131   form gaseous HNO_3 as well as nitrate aerosol (Brown & Stutz, 2012).
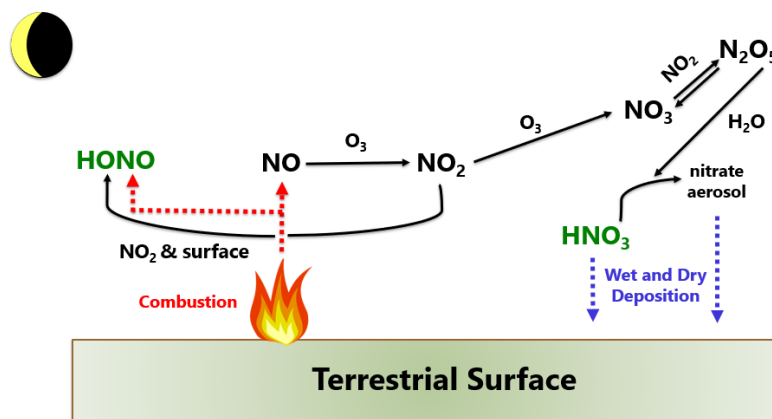

132

133   Figure 3. Summary of nocturnal pathways for reactive nitrogen in smoke plumes.

134   Here we present evidence for the secondary production of HONO in biomass burning plumes

135   and explore the surface-based pathways responsible for that production. Results are reported for

136   the Western U.S. wildfires sampled during FIREX-AQ (Figure 1) and a case study is presented

137   for the most prominent of those fires (William Flats Fire). Observations from this work are

138   crucial to understanding the evolution of wildfire-sourced reactive nitrogen, the implications for

139   air quality in the human breathing zone and highlight the importance of ground-based research

140   platforms.

141   **2. Methodology**

142   2.1 Mobile Aerosol Characterization (MACH-2) Laboratory and Sampling Logistics

143   The NASA mobile laboratory known as MACH-2 was equipped with a variety of aerosol and

144   gas phase sensors, as well as a dual mist chamber-ion chromatograph (MC/IC) system and

145   denuder collections for measurements of reactive nitrogen species. Further descriptions of the

146   MACH-2 data set are included in section 3.1. MACH-2 was initially deployed to the Boise,

147   Idaho area to sample surface level biomass burning plumes from target fires identified by

148   FIREX-AQ campaign leadership. The majority of collections were conducted at the Williams

149   Flats and Nethker fires, accounting for approximately 54% and 21% of MC/IC sampling,

150   respectively. The Williams Flats fire was by far the largest, growing to a maximum of 44,446

151   acres (Table 1). Each fire presented distinct conditions resulting from available fuels, fire state

152   (smoldering versus flaming) and sampling access. In this work the Williams Flats fire is used as

153   a case study due to the duration and continuity of sampling. Comparisons between Williams

154   Flats, Nethker and Little Bear fires are also made. Data for these fires are available in the

155   Ecosystems Burned Analysis files in the FIREX-AQ data archive (see data acknowledgment

156   below). The NASA DC-8 research aircraft, as part of FIREX-AQ, also sampled the Williams

157   Flats fire which allowed for data set comparisons between the two platforms during overlap

158   periods.

159   Table 1. MC/IC Sampling Dates, Fire Names, Approximate Locations and Maximum Burned Acreage.

Sampling Dates	Fire	Approximate Location	Max Burned Acreage
7/26 – 7/28	Shady	Challis, ID	6,286
8/2	Black Diamond	Lincoln, MT	36
8/3 – 8/7	Williams Flats	Fort Spokane, WA	44,446
8/9 – 8/16	Nethker	Burgdorf, ID	2,360
8/20 – 8/21	Little Bear	Bryce Canyon, UT	2,350

160   2.2 Nitrous and Nitric Acid Sampling Technique

161   HONO and HNO_3 concentrations were measured, in near real time, using a dual mist

162   chamber-ion chromatograph (MC/IC) system resulting in approximately 1,200 total samples. The

163   MC/IC sampling/analysis technique has been previously described in detail by Talbot et al.

164   (1997). The MC/IC was shock mounted within the NASA mobile laboratory to reduce the

165   potential for malfunctions during transits. The automated custom-built MC/IC is composed of

166   Dionex analytical components and utilizes automated syringe pumps to inject samples and

167   standards (Scheuer et al., 2003). The system is closed minimizing the potential for

168   contamination. Injection volumes were fixed at 5 mL to allow for enough sensitivity to detect the

169   targeted analytes. The use of electronic suppression via a Dionex Anion Self-Regenerating

170   Suppressor minimized the background signal. Triflouroacetate (TFA) added to the ultrapure

171   sampling water filling the MC served as an internal tracer for sample solution volumes. The

172   TFA concentration increased 10-20% due to evaporation caused by the sample air flow over a

173   300 second sample period, allowing the final sample solution volume to be amended within ±

174   3%. Between the 300 second samples there are 100 second gaps during which samples are

175   injected into the IC and the MC is refilled before the next run. The IC was calibrated on a daily

176   basis utilizing a series of eight known standards of aqueous NO_2^- and NO_3^-. Eluents are

177 maintained under a pressurized helium environment. These solutions were replenished after two

178 calibration runs. This system was utilized during the initial phase of FIREX-AQ to analyze

179 smoke during controlled laboratory studies at the FIREX-FIRELAB in the fall of 2016 (Chai et

180 al., 2019) and more recently during the 2018 collaborative WE-CAN Campaign (Chai et al.,

181 2020).

182 The mist chambers collected gas soluble samples. The sample flow was pulled into parallel

183 streams through an externally mounted Fluoropore filter by use of a scroll pump at a controlled

184 nominal rate of 35 L/min. These filters were retained for the aerosol analysis described in section

185 2.3. Samples from one mist chamber were injected into one channel of the IC for HNO_3 and

186 HONO concentration measurements. Samples from the second mist chamber were transferred

187 via a syringe pump to an amber polyethylene sample bottle to be analyzed by Brown University

188 for isotopic analysis of HNO_3 if >10 nmol of nitrate was collected.

189 2.3 Filter Sampling and Extractions

190 A total of 37 Flouropore filter samples were collected and extracted in the field to determine

191 the relative concentrations of aerosol associated ions (Cl^-, NO_3^-, SO_4^{2-}, $C_2O_4^{2-}$, Na^+, NH_4^+, K^+,

192 Mg^{2+}, Ca^{2+}). Collection times per sample ranged from 0.5 – 15 hours depending on factors such

193 as the thickness of the plume, duration of the plume and MC/IC run time. Upon removal, filters

194 were stored in a freezer for preservation until extraction in batches of 16 filters. Due to the

195 hydrophobic nature of the filters, methanol (500 µL) was used to wet the filter allowing for the

196 contents to be dissolved in deionized water (20 mL). The solutions were then transferred to

197 sample bottles and preserved via the addition of chloroform (100 µL). Concentrations of the

198 ionic species were determined using a benchtop IC at the University of New Hampshire.

199 **3. Ancillary Data Sets**

200 3.1 MACH-2

201 All real time 1 Hz data collected on MACH-2 were averaged and merged to MC/IC run times

202 accounting for the 100 second sample breaks. Gas phase data includes mixing ratios for CO and

203 NO_2. Aerosol data includes PM2.5 mass loading and aerosol optical scattering coefficients at 450

204 nm. Furthermore, an AirMar sensor logged GPS coordinates. A full list of utilized merged

205 variables, units and the instruments used for measurements relevant to this analysis are included

206 in Table 2.

207
208 Table 2. Variables, associated units and instruments used for measurements on MACH-2.

Variable	Units	Instrument
CO	ppmv	Los Gatos Research iCOS Spectrometer
NO_2	ppbv	Los Gatos Research NO_2 Spectrometer
PM2.5	$\mu g/m^3$	Teledyne T640 PM Mass Monitor
AerOpt. Scat.	Mm^{-1}	Air Photon Nephelometer (450 nm)
Lat. and Long.	Deg.	AirMar G2183 GPS Sensor

209   3.2 Physical Distances

210   The Fire to Fuels group at NASA Langley provided the position of the maximum fire

211 radiative potential (FRP) for the Williams Flats fire at the midpoint of each MC/IC sample,

212 straight-line physical distances were determined between MACH-2 logged GPS coordinates and

213 these locations of maximum FRP. FRP detections were combined from the Moderate Resolution

214 Imaging Spectroradiometer (MODIS) and Visible Infrared Imaging Radiometer Suite (VIIRS)

215 instruments. MODIS is a key instrument onboard NASA's Terra and Aqua satellites while

216 VIIRS is housed onboard the Suomi National Polar-Orbiting Partnership spacecraft.
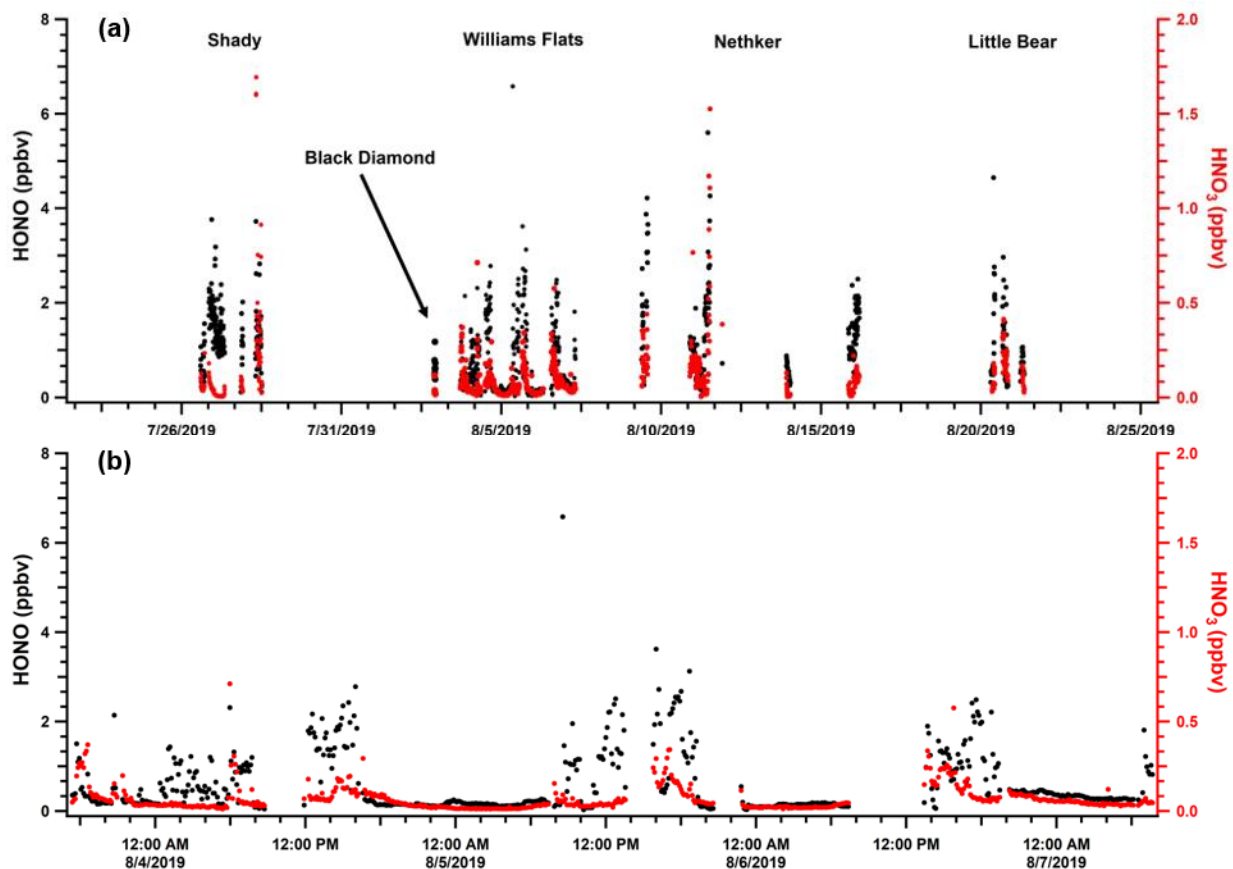
217   3.3 UV-A Irradiance

218   In situ calibrated UV-A irradiance measured by an Ultraviolet Multifilter Rotating

219 Shadowband Radiometer located in Pullman, WA approximately 65 miles from the Williams

220 Flats fire was used to determine correlations between total UV-A irradiation and HONO/NO_2.

221 Irradiance at 368 nm was used as a proxy for the full UV-A range (315 – 400 nm) which is

222 known to drive heterogenous reactions of NO_2 resulting in the production of HONO. These UV-

223 A data is publicly available as part of the Colorado State University UV-B Monitoring and

224 Research Program (Colorado State University, 2020)

225 **4. Results and Discussion**

226   4.1 HONO and HNO_3 Variations

227   Across the campaign HONO mixing ratios ranged from a minimum recorded concentration of

228 0.03 ppbv to a maximum of 6.6 ppbv with an average value of 0.9 ppbv (Figure 4a). The most

229 continuous and robust sampling was conducted at the Williams Flats fire (Figure 4b). HONO and

230 HNO_3 exhibited corresponding diurnal variability (Figure 4b). Average mixing ratios were

231 enhanced during the daytime compared to nocturnal levels at all fires where diurnal sampling

232 was conducted. Both species display greater mixing ratio variability in the daytime as a result of

233   photolytic processes and the turbidity of the convective mixed layer. The lack of photolysis and

234   convection produced much smaller and more constant mixing ratios at night. Daytime HONO

235   mixing ratios were generally an order of magnitude greater than those measured for HNO_3.This

236   matches the pathways presented in Figure 2, as HONO is directly emitted and has two expected

237   formation pathways, while BB emissions of HNO_3 are minimal and its single production

238   pathway in the atmosphere from NO_2 is outcompeted by HONO formation as the plume ages.

239   Furthermore, HNO_3 undergoes wet and dry deposition and contributes to the formation of nitrate

240   aerosol (p-NO_3^-). Analysis of filter collected NO_3^- indicates that HNO_3 partitioning favored p-

241   NO_3^- over the gas phase HNO_3 60% of the time (Figure S1). The photolysis of p-NO_3^- presents

242   another potential pathway for secondary HONO production (Ye et al., 2017). However, isotopic

243   modeling conducted by collaborators at Brown University indicates that this pathway is a minor

244   contributor to the overall HONO budget (Chai et al., 2020), thus we focus on other mechanisms

245   to explain the observations.

246   Figure 4. Timeseries of HONO and HNO_3 across the five fires sampled by the MACH-2 mobile laboratory

247   platform during the 2019 FIREX-AQ campaign (a) and expanded plot for the Williams Flats fire (b).

248
249
250
251
252
253
254
255

256   4.2 Young vs. Aged Smoke

257   A major FIREX-AQ goal was to quantify compositional differences between young and aged

258   smokes plumes. In these classifications, young plumes are more freshly emitted and aged plumes

259   correspond to a greater extent of chemical processing. A recently published paper by Selimovic

260   et al. (2020) suggests use of enhancement ratios between PM2.5 and CO as a valid method to bin

261   wildfire plume age. Applying that approach here, scatter plots of PM2.5 versus CO exhibit two

262   distinct highly linear populations for the Williams Flats, Nethker and Little Bear fires (Figure 5).

263   These differing fire conditions resulted in distinct ratios used to separate the populations. Of the

264   two, the population with the steeper slope (i.e., more PM2.5 (y-axis) loading per CO (x-axis)

265   levels) corresponds to young smoke while the other population is representative of aged smoke

266   (Figure 5a-c). The Shady fire proved to be a useful example for comparing background to smoke

267   impacts (Figure 5d). The plume from the Shady fire was very well defined and thus allowed for a

268   clean assessment of background levels which exhibit no correlation ($R^2 = 0.004$) between PM2.5

269   and CO. Once the plume front moved into the valley where we were sampling, PM2.5 was

270   elevated and is tightly correlated with CO ($R^2 = 0.90$). This divergence in correlations highlights

271   that virtually all samples taken at the Williams Flats, Nethker and Little Bear fires were smoke

272   impacted. In each case ΔPM2.5 (enhancement from background PM2.5) to ΔCO (enhancement

273   from background CO) ratios prove to be powerful metrics allowing the categorization and thus

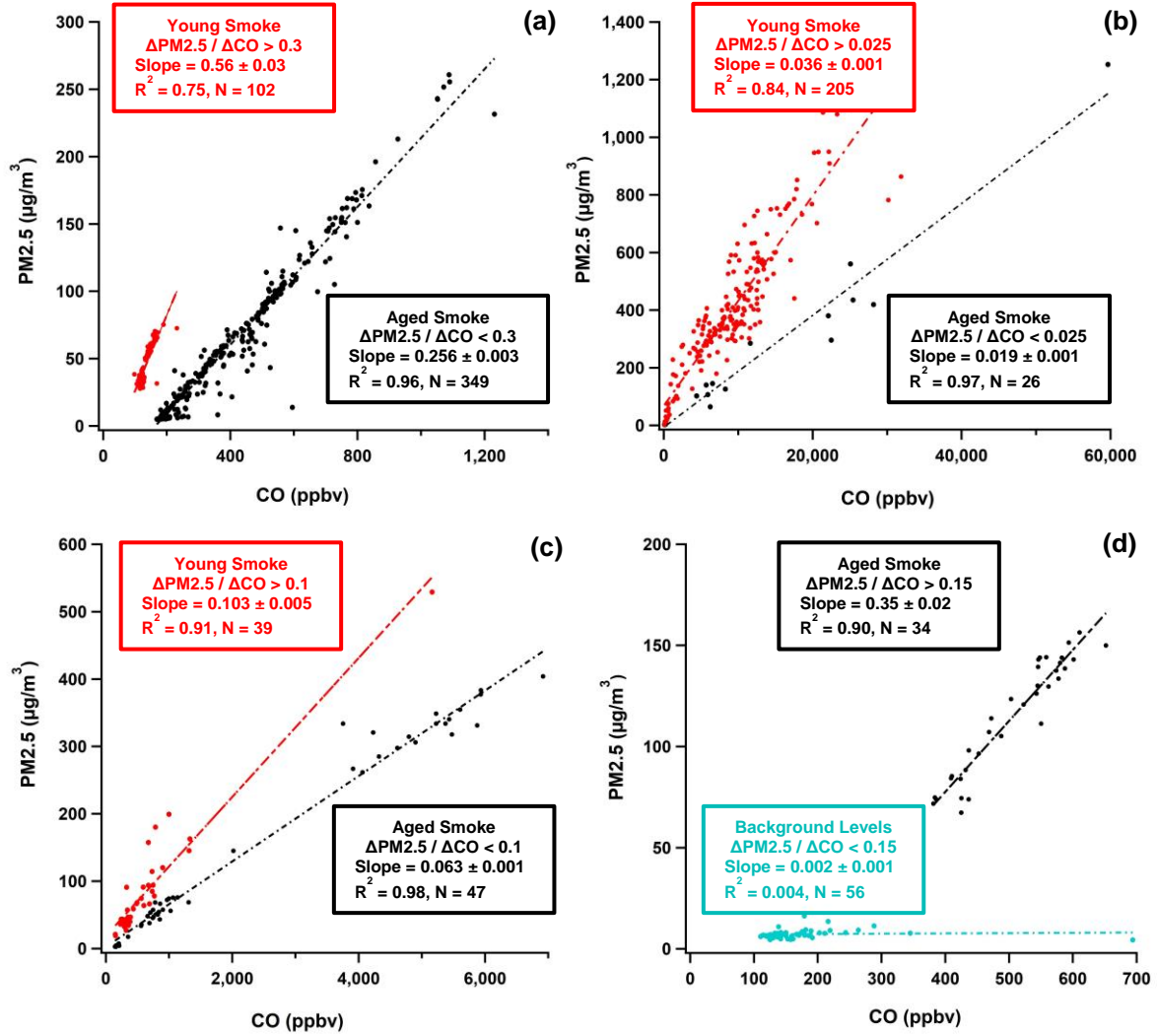274   quantification of differences present between younger and more processed plumes.

275

276

277

278

279

Figure 5. Young vs.aged ΔPM2.5/ΔCO binning for Williams Flats (a), Nethker (b), Little Bear (c) and Shady (d) fires. Williams Flats, Nethker and Little Bear all exhibit two strongly correlated populations (with the red dashed line indicative of "young" smoke and the black dashed line indicative of "aged" smoke). The Shady fire is included as an example of background levels.

283   To validate the ΔPM2.5 to ΔCO ratio as an indicator of processing, all values of the ratio

284   measured in the Williams Flats smoke plume are plotted as a function of the physical distance

285   between MACH-2 and the maximum FRP measured by MODIS and VIIRS (Figure S2). The red

286   dashed line indicates the ΔPM2.5 to ΔCO ratio of 0.3 used to distinguish young from aged smoke

287   for the Williams Flats data herein. All ratios categorized as being young were measured at a

288   straight-line distance of 8 km while those categorized as aged exceeded 10 km spanning out

289   towards 70 km at maximum. Note, the categorization between young and aged smoke is relative,

290   hence the ratio applied for this distinction varies from one fire data set to the next (Figure 5).

291

292   4.3 Implications of Secondary HONO Production

293   It is well established that the diurnal cycle impacts BB-sourced HONO concentrations.

294   Surprisingly our results indicate that for Williams Flats and Nethker young daytime smoke

295   contained significantly higher concentrations of HONO than young nighttime smoke (Figure 6a-

296   b). Higher nighttime concentrations were expected due to a lack of nocturnal HONO loss

297   pathways and the stability of the shallow nocturnal boundary layer. At Nethker, enhanced

298   HONO in young daytime smoke can be attributed to differences in fire state between day and

299   night. More flaming during the day results in proportionally greater primary HONO production.

300   This primary production was accessible to MACH-2 at the Nethker fire, as sampling occurred

301   where vegetation was actively flaming within 15 m of the mobile lab. Day/night differences for

302   the Williams Flats smoke were less obvious. In the presence of solar irradiation, primary HONO

303   has a lifetime ranging between 10 – 20 minutes (Spataro & Ianniello, 2014). At a straight-line

304   distance of 8 km the average windspeed would need to exceed 24 km/hr for primary HONO to

305   be measurable by MACH-2. Real-time weather data for the region indicates a maximum

306   recorded windspeed of 24 km/hr during the sampling period. Therefore, it is unlikely that

307   enhanced daytime primary HONO emission caused the difference at the Williams Flats fire. CO

308   observations suggest that plume thickness was the dominant factor causing the statistical

309   difference in HONO loading, as much higher CO was measured during the daytime (daytime

310   average = 368 ppbv, nighttime average = 285 ppbv).
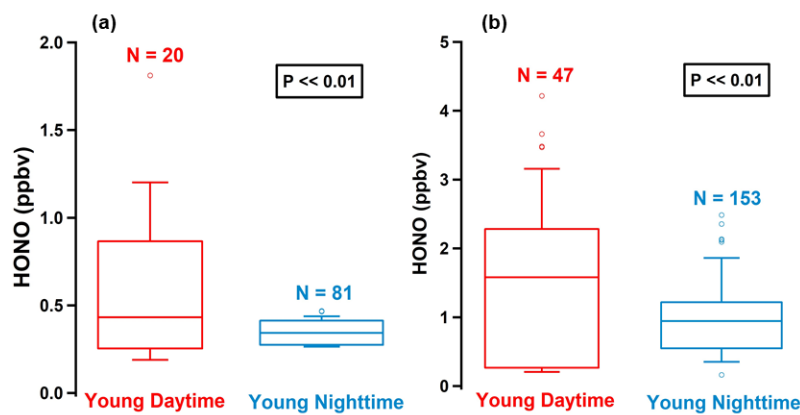
311

312

Figure 6. The impact of diurnal cycle on average HONO concentrations in young smoke plumes for the Williams Flats (a) and Nethker (b) fires. Statistical P values are based off a 95% confidence interval and N values represent population sizes.

313   The lack of statistical differences between average HONO mixing ratios in young and aged

314   smoke from a given fire is a strong indicator of substantial secondary HONO production under

315   daytime and nocturnal conditions as shown by examples from the Williams Flats and Little Bear

316   fires, given the short lifetime of HONO during both day (10-20 min) and night (1-2 hr) (Figure

317   7a-c). This ground-based observation contrasts with previous findings from airborne platforms.
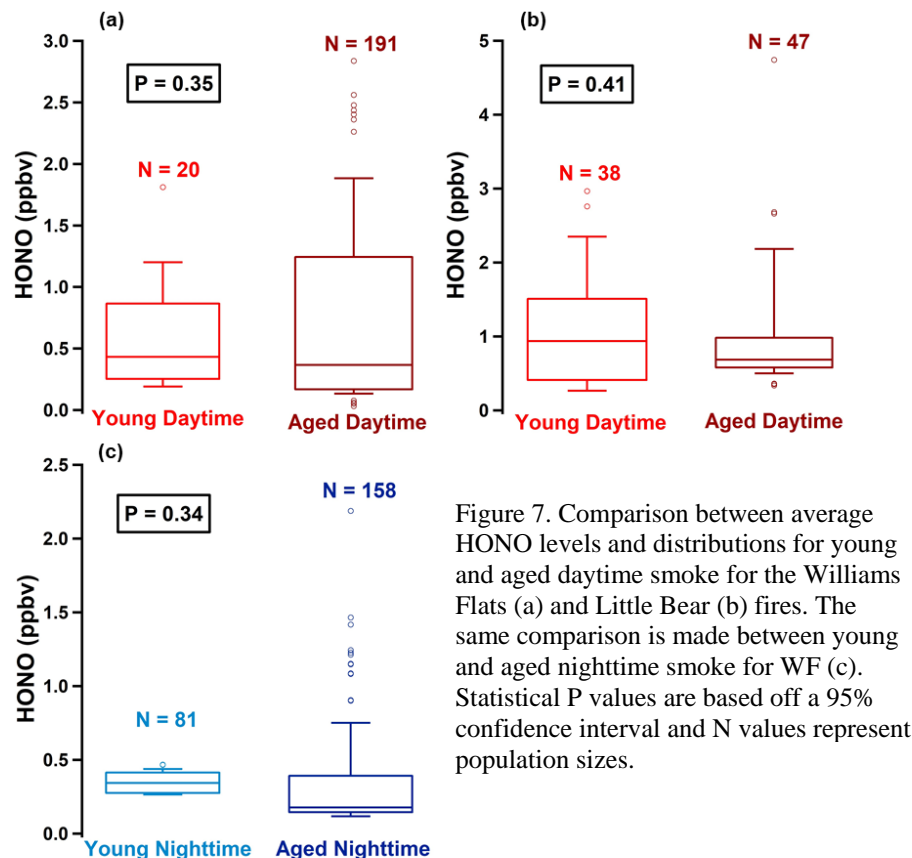

Figure 7. Comparison between average HONO levels and distributions for young and aged daytime smoke for the Williams Flats (a) and Little Bear (b) fires. The same comparison is made between young and aged nighttime smoke for WF (c). Statistical P values are based off a 95% confidence interval and N values represent population sizes.

318   No substantial evidence was found for secondary HONO production in BB plumes sampled

319   from the NOAA P3 aircraft during the Southeast Nexus Experiment (Neuman et al., 2016).

320   Interestingly, results from NASA's DC-8, which took measurements of the Williams Flats fire at

321   higher altitudes, also provide no clear evidence for substantial secondary production of HONO.

322   However, there are several factors which could contribute to the differences in the budget and

323   cycling of HONO between the ground-based MACH-2 mobile laboratory and the DC-8.

324   The atmospheric environment could be a substantial factor. In near-source plumes, which the

325   DC-8 had better access to, the conditions are NO_x limited due to a large quantity of VOCs and

326   SVOCs that store reactive nitrogen as temporary sinks. The secondary production of HONO is

327   very limited in these NO_x deficient environments and could explain why DC-8 results do not

328   indicate secondary HONO production. Stark differences in measured NO_2 mixing ratios support

329   this hypothesis (Figure S3). Furthermore, heterogenous conversion on ground surfaces (soil,

330   foliage and dust) are also suggested as dominant pathways for the secondary production of

331   HONO (see section 4.4 below). These ground-based conversions would enhance HONO levels in

332   the boundary layer airmasses sampled by MACH-2. Overall, the divergent results indicate the

333   importance of ground-based studies and present an argument for mobile laboratories to

334   collaborate with aircraft during future campaigns.

335   4.4 Influence of UV-A Solar Irradiation and Aerosol Surface Area on Heterogenous NO_2
336   to HONO Conversions

337   Heterogenous conversion of NO_2 to HONO has been represented in the literature by use of

338   HONO/NO_2 ratios (Li et al., 2012; Nie et al., 2015). The diurnal variation of these ratios exhibit

339   alignment with daily changes in UV-A solar flux across five days for the Williams Flats fire.

340   HONO/NO_2 declines in magnitude along the falling edge of UV-A on August 3rd and can be seen

341   increasing along the rising edge on the morning of August 7th with maxima aligning with peak

342   solar flux on August 5th (Figure 8a). This dependency was further probed by averaging ratios for

343   approximately 30-minute intervals across each day. The maximum 30-minute HONO/NO_2

344   average each day, which occurred at different times due to the MC/IC duty cycle, show a clear

345   dependency ($R^2 = 0.91$) on corresponding averaged UV-A flux (Figure 8b). This relationship

346   indicates that heterogenous conversions of NO_2 to HONO more than compensate for rapid

347   photolytic losses of HONO even when UV-A flux is at its highest intensity. A similar

348   observation was made in an urban setting by Wong et al. (2012) during the 2009 Study of

349   Houston Atmospheric Radical Precursor (SHARP) experiment. The resulting net HONO

350   production supports the lack of statistical differences in mean HONO mixing ratios between

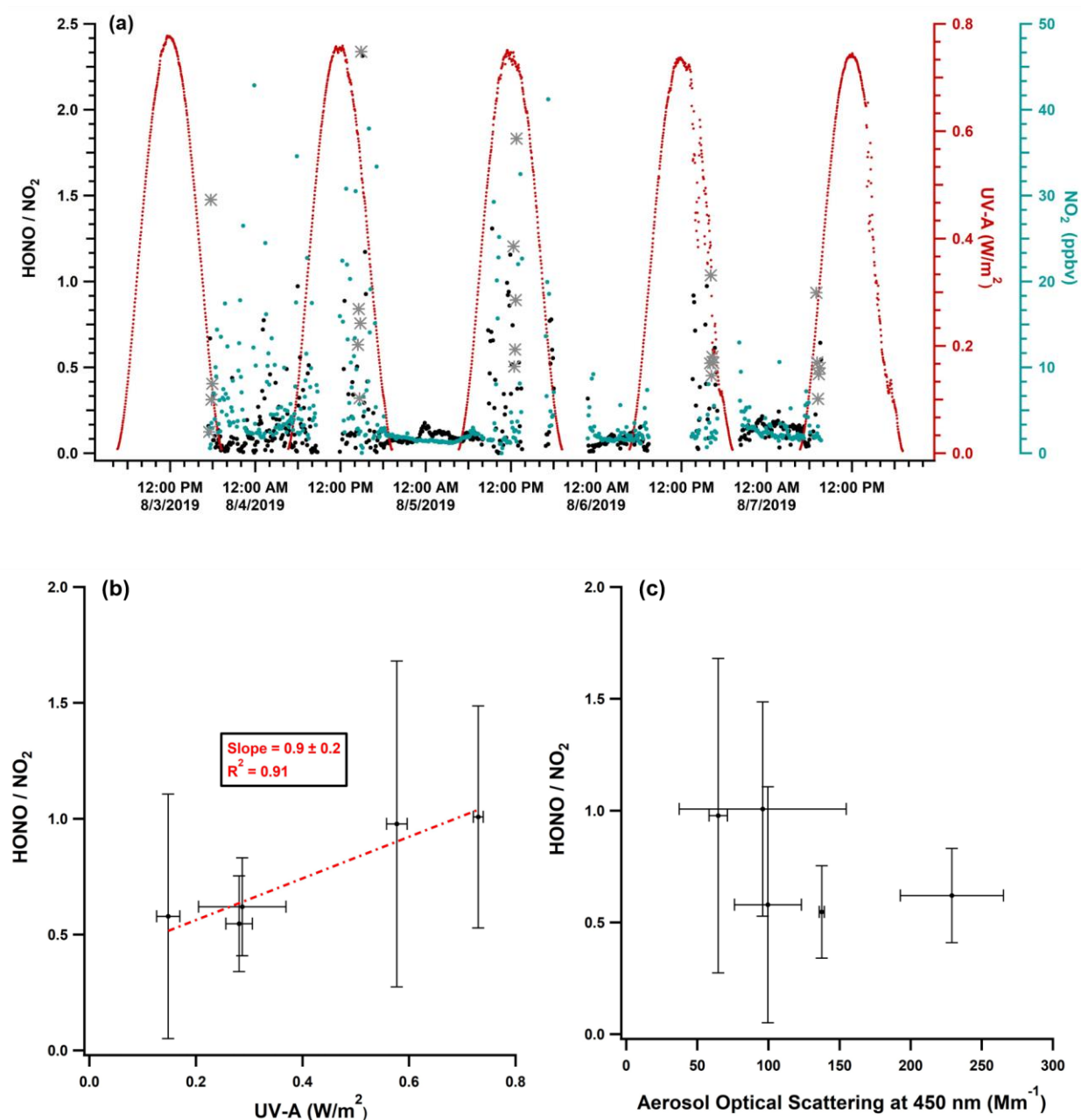351   young and aged daytime smoke for the William's Flats and Little Bear fires (Figure 7a-b).

Figure 8.Time series HONO to NO₂ ratios (left), UV-A irradiation and NO₂ mixing ratios (right) (a), as well as the dependence of those HONO to NO₂ ratios on UV-A irradiation across five daytime collection periods at the Williams Flats fire (b). The same NO₂ to HONO conversion efficiencies are also included as a function of aerosol optical scattering at 450 nm (c). The gray stars in panel (a) indicate the HONO/NO₂ data points utilized for the averaging based analysis in panels (b) and (c). Error bars represent the standard deviations (1σ) over the averaged intervals.

361   A comprehensive review of HONO sources notes that aerosols can significantly contribute to

362   the secondary production of HONO if the aerosol loading is substantial, however ground sources

363   were found to overshadow aerosol impacts in urban and forest studies (Spataro & Ianniello,

364   2014). These conversions include those from redox chemistry facilitated by quinone species

365   present in humic acid (Han et al., 2016; Scharko et al., 2017), surface reactions promoted by

366   mineral dust (Ma et al., 2013; Ndour et al., 2008; Chai et al., 2020), as well as the photolysis of

367   adsorbed nitric acid on the surface of foliage (Zhou et al., 2011). Anthropogenic surfaces could

368   also be a contributor, but those surface site reactions have not been well constrained. In contrast

369   to urban and forest environments the aerosol loading and corresponding surface area in biomass

370   burning plumes is considerably higher. Thus, the contribution of aerosol to secondary HONO

371   production was explored using the same averaging method as was done for Figure 8b. No clear

372   relationship is present between $HONO/NO_2$ and aerosol optical scattering at 450 nm, which is

373   used here as a proxy for mass loading (Figure 8c). In fact, the highest $HONO/NO_2$ ratios

374   correspond with the lowest two scattering averages. This indicates that the terrestrial surface

375   provides the vast majority of available sites facilitating the daytime heterogenous HONO

376   production. Under higher aerosol loading conditions there may be a dampening effect where

377   aerosol optical extinction limits the UV-A flux reaching the terrestrial surface, potentially

378   inhibiting the extent to which heterogenous reactions occur there. It is possible that aerosol

379   surface sites also contribute to secondary HONO production although our data did not provide

380   evidence for this. More work is required to further assess the quantitative impact of aerosol

381   loading on ground-based secondary HONO formation.

5. Conclusions

383   Over the course of FIREX-AQ, MC/IC samples collected on board NASA's MACH-2

384   provided near-real time concentrations of HONO and HNO_3 for five distinct fires in the Western

385   U.S. This variety of fires offered a chance for high-level comparisons between the

386   aforementioned species. Relative plume age was determined by use of enhancement ratios

387   between PM2.5 and CO. Average HONO concentrations were significantly higher in young

388   daytime than young nighttime smoke while no statistical differences were observed upon

389   comparing young and aged smoke. The lack of statistical differences between young and aged

390   smoke under both daytime and nocturnal conditions is evidence that substantial secondary

391   HONO production is associated with ground-level smoke plumes.

392   The Williams Flats fire presented a unique opportunity for a case study given the fire's size,

393   the extent of sampling and overlap with the DC-8 platform. Across five days, heterogeneous

394   conversions of NO_2 to HONO are strongly correlated with UV-A flux indicating that these

395   conversions, likely occurring on the ground, more than compensate for rapid photolytic losses of

396   HONO.

397   Overall, this work presents strong evidence for secondary production of HONO occurring

398   through heterogenous NO_2 surface site reactions. However, more studies utilizing ground-based

399   platforms are needed to verify whether the results from the Williams Flats fire case study are

400   universal to all wildfires. Furthermore, future collaborations between mobile laboratories such as

401   MACH-2 and aircraft will be essential for a comprehensive understanding of reactive nitrogen

402   evolution in smoke plumes and their implications for air quality.

403   **6. Data Availability Statement**

404   All data used for this analysis, except for UV-A solar irradiation, is publicly available at the

405   NASA Airborne Science Data for Atmospheric Composition database

406   (doi:10.5067/SUBORBITAL/FIREXAQ2019/DATA001). The UV-A data is publicly available

407   at the Colorado State UV-B Monitoring and Research Program.

408   **Acknowledgements**

413
414
415
416
417
418
419
420
421
422
423
424
425
426
427
428

429 **References**

430 Adon, M., Galy-Lacaux, C., Yoboue, V., Delon, C., Solmon, F., & Kaptue Tchuente, A. T.
431   (2013). Dry deposition of nitrogen compounds (NO_2, HNO_3, NH_3), sulfur dioxide and
432   ozone in West and Central African ecosystems using the inferential method. *Atmospheric*
433   *Chemistry and Physics Discussions*, *13*(5), 11689–11744. https://doi.org/10.5194/acpd-13-
434   11689-2013

435 Ainsworth, E. A., Yendrek, C. R., Sitch, S., Collins, W. J., & Emberson, L. D. (2012). The
436   effects of tropospheric ozone on net primary productivity and implications for climate
437   change. *Annual Review of Plant Biology*, *63*, 637–661. https://doi.org/10.1146/annurev-
438   arplant-042110-103829

439 Brown, S. S., & Stutz, J. (2012). Nighttime radical observations and chemistry. *Chemical Society*
440   *Reviews*, *41*(19), 6405–6447. https://doi.org/10.1039/c2cs35181a

441 Chai, J., Joyce, E., Blum, D., Bekker, C., Kaspari, J., Jordan, C., … Hastings, M. (2020),
442   Isotopically Tracking Nitrogen Oxides, Nitrous Acid, Nitric Acid, and Particulate Nitrate
443   from Wildfire during FIREX-AQ, Abstract [A-234-07] presented at 2020 Fall Meeting,
444   AGU, Online Everywhere, 1-17 December 2020.

445 Chai, J., Miller, D. J., Scheuer, E., Dibb, J., Selimovic, V., Yokelson, R., … Hastings, M. (2019).
446   Isotopic characterization of nitrogen oxides (NO_x), nitrous acid (HONO), and nitrate (NO_3^-)
447   from laboratory biomass burning during FIREX, 6303–6317. https://doi.org/10.5194/amt-
448   12-6303-2019

449 Colorado State University. UV-B Monitoring and Research Program. Retrieved from
450   https://uvb.nrel.colostate.edu/UVB/index.jsf

451 ESRL Chemical Sciences Division. (2019). FIREX-AQ Goals. Retrieved from
452   https://www.esrl.noaa.gov/csd/projects/firex-aq/science/goals.html

453 George, Christian, Ammann, M., D'Anna, B., Donaldson, D. J., & Nizkorodov, S. A. (2015).
454   Heterogeneous Photochemistry in the Atmosphere. *Chemical Reviews*, *115*(10), 4218–4258.
455   https://doi.org/10.1021/cr500648z

456 Grutzen, P. J., & Andreae, M. O. (1990). Biomass burning in the tropics: Impact on atmospheric
457   chemistry and biogeochemical cycles. *Science*, *250*(4988), 1669–1678.
458   https://doi.org/10.1126/science.250.4988.1669

459 Han, C., Yang, W., Wu, Q., Yang, H., & Xue, X. (2016). Heterogeneous Photochemical
460   Conversion of NO_2 to HONO on the Humic Acid Surface under Simulated Sunlight.
461   *Environmental Science and Technology*, *50*(10), 5017–5023.
462   https://doi.org/10.1021/acs.est.5b05101

463 Hoover, K., & Hanson, L. A. (2019). Wildfire Statistics, 3–4.

464 Li, X., Brauers, T., Häseler, R., Bohn, B., Fuchs, H., Hofzumahaus, A., … Wahner, A. (2012).
465   Exploring the atmospheric chemistry of nitrous acid (HONO) at a rural site in Southern
466   China. *Atmospheric Chemistry and Physics*, *12*(3), 1497–1513. https://doi.org/10.5194/acp-
467   12-1497-2012

468 Ma, J., Liu, Y., Han, C., Ma, Q., Liu, C., & He, H. (2013). Review of heterogeneous
469   photochemical reactions of NOy on aerosol - A possible daytime source of nitrous acid
470   (HONO) in the atmosphere. *Journal of Environmental Sciences (China)*, *25*(2), 326–334.
471   https://doi.org/10.1016/S1001-0742(12)60093-X

472

473

474

Ndour, M., D'Anna, B., George, C., Ka, O., Balkanski, Y., Kleffmann, J., … Ammann, M. (2008). Photoenhanced uptake of NO_2 on mineral dust: Laboratory experiments and model simulations. *Geophysical Research Letters*, *35*(5), 1–5. https://doi.org/10.1029/2007GL032006

Neuman, J. A., Trainer, M., Brown, S. S., Min, K., Nowak, J. B., Parrish, D. D., … Veres, P. R. (2016). HONO emission and production determined from airborne measurements over the Southeast U.S. *Journal of Geophysical Research Atmospheres*, 9237–9250. https://doi.org/10.1002/2016JD025197

Nie, W., Ding, A. J., Xie, Y. N., Xu, Z., Mao, H., Kerminen, V. M., … Fu, C. B. (2015). Influence of biomass burning plumes on HONO chemistry in eastern China. *Atmospheric Chemistry and Physics*, *15*(3), 1147–1159. https://doi.org/10.5194/acp-15-1147-2015

Nuvolone, D., Petri, D., & Voller, F. (2018). The effects of ozone on human health. *Environmental Science and Pollution Research*, *25*(9), 8074–8088. https://doi.org/10.1007/s11356-017-9239-3

Ossohou, M., Galy-Lacaux, C., Yoboué, V., Hickman, J. E., Gardrat, E., Adon, M., … Opepa, C. (2019). Trends and seasonal variability of atmospheric NO_2 and HNO_3 concentrations across three major African biomes inferred from long-term series of ground-based and satellite measurements. *Atmospheric Environment*, *207*(2), 148–166. https://doi.org/10.1016/j.atmosenv.2019.03.027

Platt, U.; Perner, D.; Harris, G. W.; Winer, A. M.; Pitts, J. N. (1980). Observations of nitrous acid in an urban atmosphere by differential optical absorption. *Nature*, *285*(5763), 312–314. https://doi.org/https://doi.org/10.1038/285312a0

Scharko, N. K., Martin, E. T., Losovyj, Y., Peters, D. G., & Ra, J. D. (2017). Evidence for Quinone Redox Chemistry Mediating Daytime and Nighttime NO_2-to-HONO Conversion on Soil Surfaces. *Environmental Science and Technology,* (2). https://doi.org/10.1021/acs.est.7b01363

Scheuer, E., Talbot, R. W., Dibb, J. E., Seid, G. K., Debell, L., & Lefer, B. (2003). Seasonal distributions of fine aerosol sulfate in the North American Arctic basin during TOPSE. *Journal of Geophysical Research*, *108*, 1–11. https://doi.org/10.1029/2001JD001364

Seinfeld, J. H., & Pandis, S. N. (2016). *Atmospheric chemistry and physics : from air pollution to climate change*.

Selimovic, V., Yokelson, R. J., McMeeking, G. R., & Coefield, S. (2020). Aerosol Mass and Optical Properties, Smoke Influence on O_3 , and High NO_3 Production Rates in a Western U.S. City Impacted by Wildfires. *Journal of Geophysical Research: Atmospheres*, *125*(16), 1–22. https://doi.org/10.1029/2020jd032791

Spataro, F., & Ianniello, A. (2014). Sources of atmospheric nitrous acid: State of the science, current research needs, and future prospects. *Journal of the Air and Waste Management Association*, *64*(11), 1232–1250. https://doi.org/10.1080/10962247.2014.952846

Stutz, J., Alicke, B., Ackerman, R., Geyer, A., Wang, S., White, A. B., … Fast, J. D. (2004). Relative humidity dependence of HONO chemistry in urban areas. *Journal of Geophysical Research: Atmospheres*, *109*(3). https://doi.org/10.1029/2003jd004135

Talbot, R. W., Scheuer, E. M., Lefer, B. L., & Luke, W. T. (1997). Measurements of sulfur dioxide during GASIE with the mist chamber technique. *Journal of Geophysical Research Atmospheres*, *102*(13), 16273–16278. https://doi.org/10.1029/97jd00132

Warneke, C., Roberts, J. M., Shwarz, J. P., Yokelson, R., & Pierce, B. (2015). *Fire Influence on Regional and Global Enviorments Experiment (FIREX) Motivations and Objectives*.

522 Wong, K. W., Tsai, C., Lefer, B., Haman, C., Grossberg, N., Brune, W. H., … Stutz, J. (2012).
523   Daytime HONO vertical gradients during SHARP 2009 in Houston , TX. *Atmospheric*
524   *Chemistry and Physics*, (2), 635–652. https://doi.org/10.5194/acp-12-635-2012
525 Ye, C., Zhang, N., Gao, H., & Zhou, X. (2017). Photolysis of Particulate Nitrate as a Source of
526   HONO and NOx. *Environmental Science and Technology*, *51*(12), 6849–6856.
527   https://doi.org/10.1021/acs.est.7b00387
528 Zhou, X., Zhang, N., Teravest, M., Tang, D., Hou, J., Bertman, S., … Stevens, P. S. (2011).
529   Nitric acid photolysis on forest canopy surface as a source for tropospheric nitrous acid.
530   *Nature Geoscience*, *4*(7), 440–443. https://doi.org/10.1038/ngeo1164
531
532